Article

Molecular Chemistry in a Zeolite: Genesis of a Zeolite Y-Supported Ruthenium Complex Catalyst

Isao Ogino, and Bruce C. Gates

J. Am. Chem. Soc., **2008**, 130 (40), 13338-13346 • DOI: 10.1021/ja804265r • Publication Date (Web): 12 September 2008

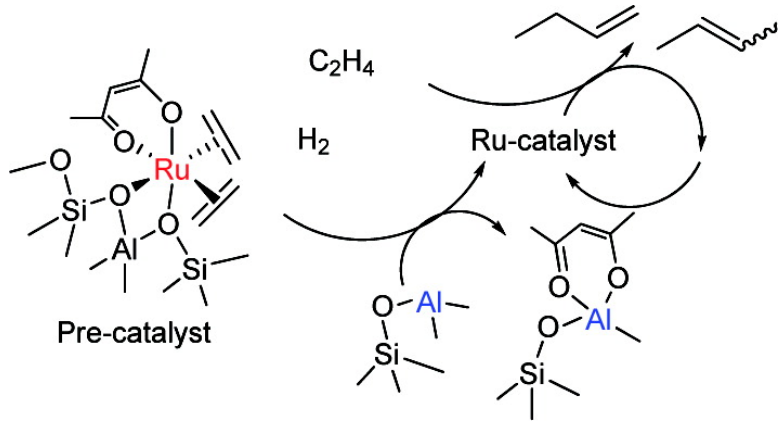

More About This Article

Additional resources and features associated with this article are available within the HTML version:

- Supporting Information
- Access to high resolution figures
- Links to articles and content related to this article
- Copyright permission to reproduce figures and/or text from this article

View the Full Text HTML

J|A|C|S
ARTICLES

Published on Web 09/12/2008

Molecular Chemistry in a Zeolite: Genesis of a Zeolite Y-Supported Ruthenium Complex Catalyst

Isao Ogino and Bruce C. Gates*

Department of Chemical Engineering and Materials Science, University of California, Davis, California 95616

Received June 5, 2008; E-mail: bcgates@ucdavis.edu

Abstract: Dealuminated zeolite Y was used as a crystalline support for a mononuclear ruthenium complex synthesized from *cis*-$Ru(acac)_2(C_2H_4)_2$. Infrared (IR) and extended X-ray absorption fine structure spectra indicated that the surface species were mononuclear ruthenium complexes, $Ru(acac)(C_2H_4)_2^{2+}$, tightly bonded to the surface by two Ru−O bonds at Al^{3+} sites of the zeolite. The maximum loading of the anchored ruthenium complexes was one complex per two Al^{3+} sites; at higher loadings, some of the *cis*-$Ru(acac)_2(C_2H_4)_2$ was physisorbed. In the presence of ethylene and H_2, the surface-bound species entered into a catalytic cycle for ethylene dimerization and operated stably. IR data showed that at the start of the catalytic reaction, the acac ligand of the $Ru(acac)(C_2H_4)_2^{2+}$ species was dissociated and captured by an Al^{3+} site. Ethylene dimerization proceeded ~600 times faster with a cofeed of ethylene and H_2 than without H_2. These results provide evidence of the importance of the cooperation of the Al^{3+} sites in the zeolite and the H_2 in the feed for the genesis of the catalytically active species. The results presented here demonstrate the usefulness of dealuminated zeolite Y as a nearly uniform support that allows precise synthesis of supported catalysts and detailed elucidation of their structures.

Introduction

Supported catalysts that are molecular analogues[1−5] find industrial application in processes such as alkene polymerization[6] and methanol carbonylation.[7] They offer opportunities for tailoring of properties by taking advantage of the structure of the support to control access to catalytic sites.[3,8,9] When such catalysts are uniform in structure, they offer the prospective advantages of molecular catalysts in solution, including high selectivity, combined with those of solid catalysts generally, such as ease of separation from products and lack of corrosion.

Zeolite supports, which are crystalline and offer well-defined bonding sites for cationic metal complexes, are appealing because of the prospects they offer for synthesis of unique supported species, as illustrated in work with a rhodium complex synthesized from $Rh(acac)(C_2H_4)_2$ (acac = $C_5H_7O_2^-$) on dealuminated zeolite Y. The supported complex was shown by temperature-dependent ^{13}C NMR spectroscopy to meet a high standard of uniformity[10] and to catalyze ethylene hydrogenation[11] and acetylene cyclotrimerization.[12]

Like mononuclear rhodium complexes, mononuclear ruthenium complexes are catalysts for numerous reactions in solution,[13] including olefin metathesis,[14−16] hydrogenation,[17] asymmetric hydrogenation,[18,19] oxidation,[20] C−C bond formation,[21,22] and activation of CO_2[23] and C−H bonds.[24] The rich catalytic chemistry of mononuclear ruthenium complexes has motivated many researchers to anchor them to solid supports, typically

(1) Guzman, J.; Gates, B. C. *Dalton Trans.* **2003**, 3303.
(2) Fierro-Gonzalez, J. C.; Kuba, S.; Hao, Y.; Gates, B. C. *J. Phys. Chem. B* **2006**, *110*, 13326.
(3) Corma, A. *Catal. Rev. Sci. Eng.* **2004**, *46*, 369.
(4) Tada, M.; Iwasawa, Y. *Chem. Commun.* **2006**, 2833.
(5) *Surface and Interfacial Organometallic Chemistry and Catalysis*; Copéret, C., Chaudret, B., Eds.; Topics in Organometallic Chemistry, Vol. 16; Springer: Berlin, 2005.
(6) Hlatky, G. G. *Chem. Rev.* **2000**, *100*, 1347.
(7) Yoneda, N.; Kusano, S.; Yasui, M.; Pujado, P.; Wilcher, S. *Appl. Catal., A* **2001**, *221*, 253.
(8) Notestein, J. M.; Solovyov, A.; Andrini, L. R.; Requejo, F. G.; Katz, A.; Iglesia, E. *J. Am. Chem. Soc.* **2007**, *129*, 15585.
(9) Hicks, J. C.; Mullis, B. A.; Jones, C. W. *J. Am. Chem. Soc.* **2007**, *129*, 8426.
(10) Ehresmann, J. O.; Kletnieks, P. W.; Liang, A.; Bhirud, V. A.; Bagatchenko, O. P.; Lee, E. J.; Klaric, M.; Gates, B. C.; Haw, J. F. *Angew. Chem., Int. Ed.* **2006**, *45*, 574.
(11) Liang, A. J.; Bhirud, V. A.; Ehresmann, J. O.; Kletnieks, P. W.; Haw, J. F.; Gates, B. C. *J. Phys. Chem. B* **2005**, *109*, 24236.
(12) Kletnieks, P. W.; Liang, A. J.; Craciun, R.; Ehresmann, J. O.; Marcus, D. M.; Bhirud, V. A.; Klaric, M. M.; Haymann, M. J.; Guenther, D. R.; Bagatchenko, O. P.; Dixon, D. A.; Gates, B. C.; Haw, J. F. *Chem.—Eur. J.* **2007**, *13*, 7294.
(13) Murahashi, S. *Ruthenium in Organic Synthesis*; Wiley-VCH: Weinheim, Germany, 2004.
(14) Trnka, T. M.; Grubbs, R. H. *Acc. Chem. Res.* **2001**, *34*, 18.
(15) Grubbs, R. H. *Angew. Chem., Int. Ed.* **2006**, *45*, 3760.
(16) Nguyen, S. T.; Grubbs, R. H.; Ziller, J. W. *J. Am. Chem. Soc.* **1993**, *115*, 9858.
(17) Evans, D.; Osborn, J. A.; Jardine, F. H.; Wilkinson, G. *Nature* **1965**, *208*, 1203.
(18) Noyori, R.; Hashiguchi, S. *Acc. Chem. Res.* **1997**, *30*, 97.
(19) Noyori, R. *Angew. Chem., Int. Ed.* **2002**, *41*, 2008.
(20) Thompson, M. S.; Meyer, T. J. *J. Am. Chem. Soc.* **1982**, *104*, 4106.
(21) Trost, B. M.; Toste, F. D.; Pinkerton, A. B. *Chem. Rev.* **2001**, *101*, 2067.
(22) Kondo, T.; Takagi, D.; Tsujita, H.; Ura, Y.; Wada, K.; Mitsudo, T. *Angew. Chem., Int. Ed.* **2007**, *46*, 5958.
(23) Jessop, P. G.; Ikariya, T.; Noyori, R. *Nature* **1994**, *368*, 231.
(24) Murai, S.; Kakiuchi, F.; Sekine, S.; Tanaka, Y.; Kamatani, A.; Sonoda, M.; Chatani, N. *Nature* **1993**, *366*, 529.

10.1021/ja804265r CCC: $40.75

metal oxides.[25−27] However, there is still a lack of examples providing key structural information about such catalysts, including details concerning metal−support bonding. This limitation is a reflection of the nonuniformity of the structures, particularly that of the support surfaces.

In the present work, we have demonstrated that dealuminated zeolite Y is an excellent support for ruthenium complex catalysts and taken advantage of the uniformity of the zeolite to elucidate the catalyst structure in detail. The catalyst was synthesized by reaction of *cis*-$Ru(acac)_2(C_2H_4)_2$[28] (**I**) with the zeolite and its structure characterized by infrared (IR) and extended X-ray absorption fine structure (EXAFS) spectroscopies. The complex enters into a catalytic cycle for ethylene dimerization, aided by H_2; the zeolite surface facilitates the genesis of the catalytically active species.

Results

Synthesis of the Precursor I. The orange-colored crystals were obtained in 43% yield by a reported method.[28]

Characterization of Surface Species Formed by Reaction of Complex I with the Zeolite. Observations during the Synthesis. The color of the synthesis mixture initially containing the zeolite and precursor **I** changed from yellow to dark-orange within a few hours after the start of mixing. After 18 h, the solution had become colorless, consistent with the complete uptake of **I** by the zeolite, corresponding to approximately one Ru atom per unit cell of the zeolite (approximately one Ru atom per eight zeolite supercages) and a Ru/Al atomic ratio of ∼1/6. Removal of the solvent by evacuation gave a solid with a light-pink color. Evidently, the ruthenium was bonded to the zeolite. The as-prepared sample was designated as Sample 1.

IR Evidence for Reaction of Zeolite Silanol Groups with I. The IR spectra indicated the presence of terminal (3743 cm^{-1}) and acidic (3629 and 3565 cm^{-1}) silanol groups in the calcined zeolite.[29] The bands characteristic of acidic silanol groups decreased significantly in intensity relative to those of the bare zeolite upon chemisorption of **I**, indicating reaction of these silanol groups in the chemisorption process (Figure 1).[30] The band at 3629 cm^{-1} was assigned to OH groups within the zeolite supercages.[29,31] The critical diameter of the precursor, ∼7 Å,[28] was small enough to allow passage of **I** through the zeolite apertures and into the supercages, where it reacted with the OH groups. The other OH band, at 3565 cm^{-1}, is representative of groups located within the smaller zeolite β-cages, which were inaccessible to the precursor.[29,31] The decrease in the intensity of this band thus suggests that ligands dissociated from ruthenium in **I** reacted with these sites.

IR Evidence of Hydrocarbon Ligands on Sample 1. The IR spectrum of Sample 1 included bands in the C−H stretching region (Figure 2). The interpretation of the spectrum was complicated by the possible overlap of bands due to ligands on the complex with C−H vibrational bands characterizing the acac ligands or species formed from them, which could either be retained by ruthenium centers or dissociated and bonded at aluminum sites in the zeolite.

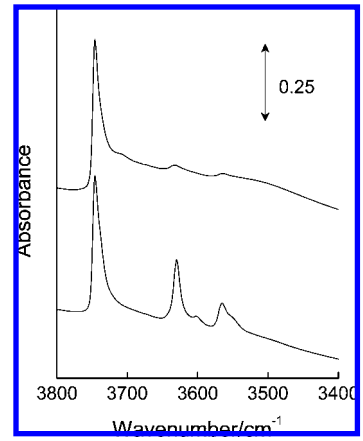

Figure 1. IR spectra of calcined dealuminated zeolite HY (lower spectrum) and the supported ruthenium complex, Sample 1 (upper spectrum).

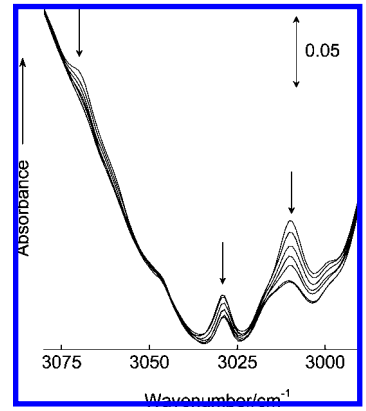

Figure 2. IR spectra of Sample 1 in 50% H_2 in He flowing at room temperature. The top spectrum corresponds to the sample before the treatment in H_2. The arrows indicate the directional changes of the absorbance as a function of time.

Reactions of Sample 1 with H_2 and D_2. IR spectra were recorded during the treatments to investigate the reactions of Sample 1 (∼30 mg) with H_2 (50% H_2 in He flowing at a total rate of 100 mL/min at room temperature and atmospheric pressure) or a pulse of D_2 (∼5 mL in He flowing at 100 mL/min at room temperature and atmospheric pressure). The data helped clarify the identifications of the bands in the C−H stretching region.

The spectra of the H_2-treated sample showed that C−H stretching bands inferred to be evidence of ethylene ligands (3010, 3030, and 3069 cm^{-1}) decreased in intensity during the treatment but did not disappear (Figure 2).[32] In the experiments using D_2 instead of H_2, the intensity of the deuterated ethane ($C_2H_4D_2^+$) peak at m/z 32 increased after the beginning of the flow of D_2 (see Figure 3S in the Supporting Information; this peak was undetectable in the mass spectra observed during H_2 flow); simultaneously, the peaks at 3010, 3030, and 3069 cm^{-1}

(25) Kaplan, A. W.; Bergman, R. G. *Organometallics* **1998**, *17*, 5072.
(26) Brühwiler, D.; Frei, H. *J. Phys. Chem. B* **2003**, *107*, 8547.
(27) Yamaguchi, K.; Mori, K.; Mizugaki, T.; Ebitani, K.; Kaneda, K. *J. Am. Chem. Soc.* **2000**, *122*, 7144.
(28) Bennett, M. A.; Byrnes, M. J.; Willis, A. C. *Organometallics* **2003**, *22*, 1018.
(29) Breck, D. W. *Zeolite Molecular Sieves: Structure, Chemistry, and Use*; Wiley: New York, 1973.
(30) Miessner, H.; Burkhardt, I.; Gutschick, D.; Zecchina, A.; Morterra, C.; Spoto, G. *J. Chem. Soc., Faraday Trans.* **1989**, *85*, 2113.
(31) Jacobs, P. A.; Uytterhoeven, J. B. *J. Chem. Soc., Faraday Trans.* **1973**, *69*, 359.

(32) Analysis of the gas-phase products by mass spectrometry was inconclusive because the peaks in the mass spectra were broad and small and the interpretation was complicated by traces of *n*-pentane solvent from the synthesis that desorbed slowly.

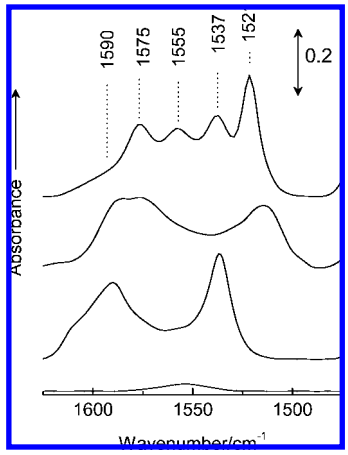

Figure 3. IR spectra of (from bottom to top) calcined dealuminated zeolite HY, acetylacetone adsorbed on the calcined zeolite, $Ru(acac)_2(C_2H_4)_2$, and Sample 1.

corresponding to C−H vibrations declined in intensity and disappeared (data not shown), confirming that they indicate π-bonded ethylene ligands on the ruthenium.[33] This result was supported by the presence of a small band at 1278 cm^{-1} in the spectrum of Sample 1 that could be assigned to the C═C stretching mode coupled with the scissor mode of CH_2 in ethylene π-bonded to Ru (data not shown).[34−37] The band appeared to be small because intense bands characteristic of the zeolite framework overlap it. The IR results were further supported by the EXAFS results presented below, which indicated a Ru−C coordination number of ∼4 (two ethylene ligands per Ru atom) and an average Ru−C distance corresponding to that of ethylene π-bonded to Ru.

Reaction of Acetylacetonate Ligands on Ruthenium. IR spectra characterizing the sample formed by adsorption of acetylacetone ($C_5H_8O_2$) on the calcined zeolite (Figure 3) included bands centered at 1537 and 1590 cm^{-1} [similar to those characterizing $Al(acac)_3$ (1534 cm^{-1})[38]] that were assigned to acetylacetonate bonded to aluminum sites in the zeolite.

The IR spectrum characterizing Sample 1 included bands at 1521, 1537, 1555, and 1575 cm^{-1}, with a small shoulder at ∼1590 cm^{-1}. The peak at 1515 cm^{-1} in the spectrum of **I**, characteristic of $\nu_{as}(CCC)_{ring}$ in the acac ligands, shifted to 1521 cm^{-1} when **I** was adsorbed. A similar band shift was observed when $Ru(acac)_3$ was adsorbed on the zeolite (Figure 4S in the Supporting Information). The 1521 cm^{-1} band characterizing Sample 1 was thus assigned to $\nu_{as}(CCC)_{ring}$ associated with the acac ligands remaining on the ruthenium.[39−41] On the basis of IR spectra characterizing the sample prepared by adsorption of acetylacetone on the zeolite,[38,42] the new band at 1537 cm^{-1} in the spectrum of Sample 1 was assigned to acac ligands dissociated from ruthenium and bonded to zeolite Al^{3+} sites.

The bands at 1555 cm^{-1} and 1575 cm^{-1} in the spectrum of Sample 1 were assigned to $2[\gamma(C-H)]$ and $\nu_s(CO)_{ring}$ of acac ligands bonded to Ru.[38,43] By comparing the IR spectrum of Sample 1 with literature data[44] and the spectrum of the zeolite with that of adsorbed acetylacetonate, we were able to assign the shoulder at 1590 cm^{-1} to $\nu_s(CO)_{ring}$ of acac ligands coordinated to Al^{3+} sites. This assignment was supported by the lack of this band in the spectrum of a silica-supported ruthenium complex sample (Figure 5S in the Supporting Information).

In summary, the IR data show that some of the acac ligands in the precursor were dissociated from ruthenium upon adsorption of **I** and became bonded to Al^{3+} sites in the zeolite. To estimate the number of acac ligands dissociated from the ruthenium in Sample 1, peak deconvolution of the IR spectra was performed, and the Ru−acac/Al−acac area ratio was determined (Figure 10S in the Supporting Information). Samples with higher ruthenium loadings (2 and 3 wt % Ru) were also investigated and found to have smaller Al−acac/Ru−acac area ratios than the sample containing only 1 wt % Ru (Figures 11S−13S in the Supporting Information); this provided a basis for identification of the ruthenium complexes in the samples, as described in the Discussion.

Further Evidence of Ligands on the Supported Mononuclear Ruthenium Complex. Sample 1 was also characterized by Ru K-edge EXAFS spectroscopy, as summarized in the following section, which includes a summary of all of the structural models considered in the EXAFS data fitting. The EXAFS results were consistent with the IR spectra, showing that the supported complex was mononuclear and bonded to the surface of the zeolite with the ethylene ligands intact; structural details are given after the following section on data analysis.

EXAFS Characterization of the Supported Mononuclear Ruthenium Complex: Data Analysis. Figure 4A shows k^2-weighted EXAFS data characterizing Sample 1 and the best fit described below. Figure 4B−D shows Fourier transforms (FTs) of EXAFS data with various k-weightings together with the best fits. Table 1 lists the six plausible structural models of the surface species that were constructed on the basis of the data presented above.

An assessment of the various candidate models is presented below and summarized in Table 2; comments about each model that was tested and an explanation of why all but one of the models were rejected are provided. The model that gave the best fit consisted of a mononuclear ruthenium complex with two ethylene ligands and with one of the two acac ligands in **I** replaced by zeolite oxygen atoms at the acidic sites near Al^{3+}, as shown below. An assessment of

(33) The spectrum reported for a supported sample prepared from $Rh(C_2H_4)_2(acac)$ and zeolite Y similarly included a peak at 3069 cm^{-1} attributed to π-bonded ethylene ligands.[11]

(34) Nakamoto, K. *Infrared and Raman Spectra of Inorganic and Coordination Compounds*, 5th ed.; Wiley: New York, 1997; Part B, p 278.
(35) Mohsin, S. B.; Trenary, M.; Robota, H. J. *J. Phys. Chem.* **1988**, *92*, 5229.
(36) Chesters, M. A.; De La Cruz, C.; Gardner, P.; McCash, E. M.; Pudney, P.; Shahid, G.; Shepppard, M. *J. Chem. Soc., Faraday Trans.* **1990**, *86*, 2757.
(37) De La Cruz, C.; Sheppard, N. *J. Chem. Soc., Faraday Trans.* **1997**, *93*, 3569.
(38) Guzman, J.; Gates, B. C. *Langmuir* **2003**, *19*, 3897.
(39) Mikami, M.; Nakagawa, I.; Shimanouchi, T. *Spectrochim. Acta, Part A* **1967**, *23*, 1037.
(40) Nakamoto, K. *Infrared and Raman Spectra of Inorganic and Coordination Compounds*, 5th ed.; Wiley: New York, 1997; Part B, p 91.
(41) Van Der Voort, P.; van Welzenis, R.; de Ridder, M.; Brongersma, H. H.; Baltes, M.; Mathieu, M.; van de Ven, P. C.; Vansant, E. F. *Langmuir* **2002**, *18*, 4420.
(42) To check the assignment, control experiments were done with pure silica as a support. The IR spectrum of the supported sample (Figure 5S in the Supporting Information) included the band at 1521 cm^{-1} assigned to acac ligands on ruthenium but not that at 1537 cm^{-1} assigned to acac ligands bonded to Al^{3+}, consistent with the lack of Al^{3+} sites on the silica.
(43) Van der Voort, P.; Mitchell, M. B.; Vansant, E. F.; White, M. G. *Interface Sci.* **1997**, *5*, 169.
(44) Baltes, M.; Van Der Voort, P.; Weckhuysen, B. M.; Rao, R. R.; Catana, G.; Schoonheydt, R. A.; Vansant, E. F. *Phys. Chem. Chem. Phys.* **2000**, *2*, 2673.

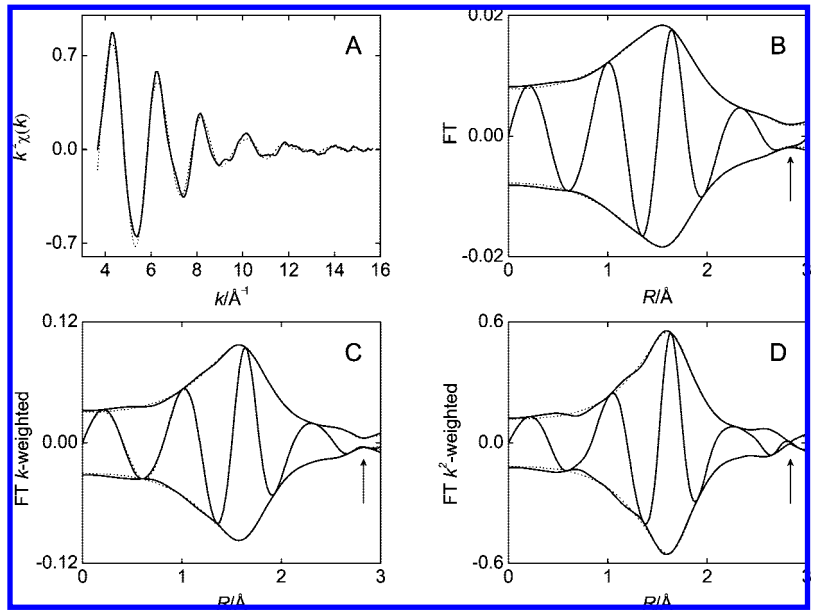

Figure 4. EXAFS data and corresponding FT magnitudes and imaginary parts characterizing Sample 1 ($\Delta k = 3.67-15.63$ Å^{-1}, $\Delta R = 0.8-3.0$ Å, phase-uncorrected): (A) k^2-weighted EXAFS data, (B) k^0-weighted FT, (C) k^1-weighted FT, and (D) k^2-weighted FT. The solid lines represent data and the dotted lines represent fits. The arrows in (B−D) indicate a constructive/destructive feature attributed to the presence of the various shells.

Table 1. EXAFS Parameters Corresponding to the Six Candidate Models Characterizing Sample 1[a]

						fit variances		
model	backscatterer	N	$10^3\Delta\sigma^2$ (Å^2)	R (Å)	ΔE_0 (eV)	Abs	Im	ε_v^2
A	O	4.0 ± 0.2	7.0 ± 0.3	2.08 ± 0.01	−3.0 ± 0.6	k^0: 0.017	k^0: 0.043	19.6
	C	4.3 ± 0.5	7.4 ± 0.5	2.22 ± 0.01	4.4 ± 0.7	k^2: 0.115	k^2: 0.255	
	Ru	3.0 ± 1.2	28 ± 4.2	3.04 ± 0.02	6.5 ± 1.3			
B	O	4.0 ± 0.3	7.1 ± 0.4	2.06 ± 0.01	0.4 ± 0.6	k^0: 0.020	k^0: 0.041	22.9
	C	4.0 ± 0.5	6.0 ± 0.6	2.20 ± 0.01	7.9 ± 1.0	k^2: 0.133	k^2: 0.331	
	Al	1.4 ± 0.6	19 ± 5	3.07 ± 0.02	0.1 ± 2.0			
C	O	4.0 ± 0.2	7.1 ± 0.3	2.07 ± 0.01	−1.7 ± 0.5	k^0: 0.009	k^0: 0.020	17.6
	C	4.3 ± 0.5	7.3 ± 0.7	2.21 ± 0.01	5.2 ± 1.0	k^2: 0.059	k^2: 0.129	
	C_l	1.8 ± 0.3	5.0 ± 0.5	3.31 ± 0.01	−8.5 ± 2.2			
D	O	4.0 ± 0.3	7.3 ± 0.4	2.07 ± 0.01	−1.1 ± 0.6	k^0: 0.009	k^0: 0.014	25.5
	C	4.4 ± 0.6	7.7 ± 0.8	2.21 ± 0.01	5.5 ± 1.2	k^2: 0.059	k^2: 0.125	
	Ru	1.7 ± 0.7	25 ± 4	2.89 ± 0.02	−14 ± 3			
	Al	0.6 ± 0.2	3.2 ± 1.0	3.21 ± 0.01	−19 ± 2			
E	O	4.0 ± 0.3	7.2 ± 0.3	2.07 ± 0.01	−1.5 ± 0.6	k^0: 0.010	k^0: 0.019	18.0
	C	4.4 ± 0.6	7.7 ± 0.8	2.22 ± 0.01	4.9 ± 1.1	k^2: 0.053	k^2: 0.119	
	C_l	2.1 ± 1.2	10 ± 60	3.05 ± 0.03	11 ± 4			
	Ru	0.8 ± 1.1	11 ± 13	3.08 ± 0.01	4.0 ± 2.1			
F	O	4.0 ± 0.3	7.1 ± 0.3	2.07 ± 0.01	−1.6 ± 0.6	k^0: 0.013	k^0: 0.015	20.6
	C	4.3 ± 0.6	7.4 ± 0.7	2.21 ± 0.01	5.1 ± 0.7	k^2: 0.053	k^2: 0.135	
	C_l	1.9 ± 0.6	3.9 ± 1.1	3.03 ± 0.02	−1.2 ± 1.3			
	Al	1.1 ± 0.2	5.4 ± 1.9	3.08 ± 0.01	1.6 ± 1.0			

[a] Fit details: R space, $3.67 < k < 15.63$ Å^{-1}, $0.8 < R < 3.0$ Å. Notation: N, coordination number; R, interatomic distance; $\Delta\sigma^2$, Debye−Waller parameter; ΔE_0, inner potential correction; Abs, real part of the FT; Im, imaginary part of the FT; ε_v^2, goodness-of-fit parameter; k^n, weighting in the Fourier transform.

the model is given in the Discussion. Details of the fitting process and selection of the model are given in the following paragraphs and in the Supporting Information.

Details of the EXAFS Data Fitting and Selection of the Model. No fit determined with only two shells was adequate, as shown by the poor agreement between the data and the best fits. Consequently, two-shell models are not considered further here. Each of the models considered in detail (three- and four-shell models) included both Ru−O and Ru−C contributions. The number of parameters used in fitting the data to each model (12 or 16) was always less than the statistically justified number (18) computed using the Nyquist theorem.[45]

Metal−light-atom backscatterer contributions such as Ru−C and Ru−O cannot generally be distinguished with confidence by EXAFS spectroscopy alone, but the IR and mass spectrometry data provided the basis for the discrimination, demonstrating

(45) Lytle, F. W.; Sayers, D. E.; Stern, E. A. *Phys. B* **1989**, *158*, 701.

Table 2. Qualitative Summary of EXAFS Fitting Results for the Six Candidate Models Representing Sample 1

model	absorber/backscatterer contributions	comments regarding quality of fit of EXAFS data to the model
A	Ru−O, Ru−C, Ru−Ru	physically unrealistically large parameter value ($\Delta\sigma^2 = 28 \times 10^{-3}$ Å^2) for the Ru−Ru contribution; individual Ru−Ru shell not fit well on application of phase and amplitude corrections
B	Ru−O, Ru−C, Ru−Al	worst values of the variances; physically unrealistically large parameter value ($\Delta\sigma^2 = 19 \times 10^{-3}$ Å^2) for the Ru−Al contribution
C	Ru−O, Ru−C, Ru−C$_l$	best goodness-of-fit value and physically realistic values for all parameters; however, individual Ru−C$_l$ shell not fit well on application of phase and amplitude corrections
D	Ru−O, Ru−C, Ru−Ru, Ru−Al	worst goodness-of-fit value; physically unrealistically large parameter values for the Ru−Ru ($\Delta\sigma^2 = 25 \times 10^{-3}$ Å^2, $\Delta E_0 = -14$ eV) and Ru−Al ($\Delta E_0 = -19$ eV) contributions
E	Ru−O, Ru−C, Ru−C$_l$, Ru−Ru	physically unrealistically large parameter values for the Ru−C$_l$ ($\Delta\sigma^2 = 10 \times 10^{-3}$ Å^2, $\Delta E_0 = 11$ eV) and Ru−Ru ($\Delta\sigma^2 = 11 \times 10^{-3}$ Å^2) contributions; individual Ru−C$_l$ and Ru−Ru shells not fit well on application of phase and amplitude corrections
F	Ru−O, Ru−C, Ru−C$_l$, Ru−Al	model providing the best fit: goodness-of-fit value within the fluctuation of that for **C**; physically realistic values for all parameters; good fit with various *k*-weightings; individual contributions fit well

the presence of ethylene ligands in the initially prepared supported ruthenium complex and their disappearance when the sample was treated with H_2 or D_2. The formation of Ru−O$_{support}$ bonds anchoring the ruthenium complex to the zeolite was suggested simply by the observation that the precursor reacted with the zeolite. Attempts to combine the Ru−O and Ru−C contributions into a single contribution in the data fitting gave an unrealistically large value of the Debye−Waller parameter $\Delta\sigma^2$ (0.015 Å^2), and the fit was judged to lack physical significance.

The six models differed from each other with regard to which of the plausible contributions (Ru−Ru, Ru−Al, and/or a second Ru−C) were included in addition to Ru−O and Ru−C. We tested for (a) a Ru−Ru contribution, in order to check for cluster formation resulting from reduction of the ruthenium (none was found); (b) a Ru−Al contribution, because of the likely reaction of the cationic ruthenium complex **I** with anionic sites in the zeolite (this contribution was found to be significant); and (c) a second Ru−C contribution (denoted Ru−C$_l$, where the "l" subscript stands for "long") arising from acac ligands on ruthenium (this was also found to be significant).

Besides the Ru−O and Ru−C contributions, the three-shell models **A**, **B**, and **C** included Ru−Ru, Ru−Al, and Ru−C$_l$ contributions, respectively. The four-shell models **D**, **E**, and **F** included Ru−Ru and Ru−Al, Ru−Ru and Ru−C$_l$, and Ru−C$_l$ and Ru−Al contributions, respectively. Addition of the third (and even the fourth) contribution led to essentially no changes in the values of the parameters characterizing the first two shells (Ru−O and Ru−C), leading us to conclude that these two contributions were significant and necessary for satisfactory modeling of the structure.

All of the models represented in Table 1 fit the overall data well, with variances well below 1%.[46] However, all of the models except **C** and **F** gave at least one physically unrealistic parameter value and thus were excluded, as summarized in Table 2 and the following paragraphs.

Each of the models **A**, **D**, and **E** included a Ru−Ru contribution. Models **A** and **D** were excluded because they gave unrealistically large $\Delta\sigma^2$ values for the Ru−Ru contribution (28×10^{-3} and 25×10^{-3} Å^2, respectively). Furthermore, the Ru−Ru contribution in **D** was characterized by an unrealistically large inner potential correction (−14 eV),[47] leading us to discard it. Model **E** gave relatively large $\Delta\sigma^2$ values for the Ru−C$_l$ and Ru−Ru contributions (10×10^{-3} and 11×10^{-3} Å^2, respectively). Furthermore, the individual contributions of these shells were not fitted well after the contributions were phase- and amplitude-corrected (Figures 6S and 7S in the Supporting Information) and the Ru−C$_l$ contribution in **E** was characterized by a large inner potential correction (>10 eV), leading to its rejection. Thus, on the basis of the analyses for models **A**, **D**, and **E**, we inferred that there was no Ru−Ru contribution (i.e., there were no clusters) that could be determined by EXAFS spectroscopy.

Model **B** included a Ru−Al contribution, for which the fit results indicated a large $\Delta\sigma^2$ value (19×10^{-3} Å^2); thus, this model lacked physical significance and was also rejected.

Inclusion of a Ru−C$_l$ contribution instead of a Ru−Al contribution (model **C**) gave the smallest value of the ε_v^2 (goodness-of-fit) parameter of all the models. However, the fit of the third-shell (Ru−C$_l$) contribution was found to be unsatisfactory after the phase and amplitude corrections were applied (Figure 8S in the Supporting Information), and thus, this model was also rejected.

Addition of a Ru−Al contribution to model **C** (to give the four-shell model **F**) gave the best fit of any of the models, and all of the parameter values were physically reasonable. This model showed good fits of all of the individual shells, as shown in Figure 9S in the Supporting Information. It also fit the data well at all of the examined *k*-weightings (k^0, k^1, and k^2), although a constructive/destructive feature was evident in the Fourier transforms (Figure 4B−D) at values of R near 2.8 Å; this observation was expected because of the presence of the various shells.[46] The addition of the Ru−Al contribution increased the goodness of fit by 17% over that of the 3-shell model **C**, but the difference of the ε_v^2 values was less than twice the value of the fluctuations in this parameter (the value of the right-hand side of eq 3 in the Supporting Information is 2).[48,49] Model **F** gave good fits of each of the individual contributions, and all of the parameter values were physically realistic (Table 1). A

(46) Koningsberger, D. C.; Mojet, B. L.; van Dorssen, G. E.; Ramaker, D. E. *Top. Catal.* **2000**, *10*, 143.

(47) Kelly, S. D.; Ravel, B. *AIP Conf. Proc.* **2007**, *882*, 132.

(48) Stern, E. A.; Newville, M.; Ravel, B.; Yacoby, Y.; Haskel, D. *Phys. B* **1995**, *209*, 117.

(49) Kelly, S. D.; Kemmer, K. M.; Fryxell, G. E.; Liu, J.; Mattigod, S. V.; Ferris, K. F. *J. Phys. Chem. B* **2001**, *105*, 6337.

clear result is that the EXAFS data demonstrated the existence of a Ru−O and two Ru−C contributions.

Thus, Model F was judged to provide the best fit of the data and is recommended. According to this model, the supported mononuclear ruthenium complex is characterized by Ru−O and Ru−C contributions at distances of 2.07 and 2.21 Å, respectively. The former agrees with the range of values determined crystallographically for the precursor complex **I** (2.055−2.080 Å).[28] The Ru−O coordination number of ∼4 accounts for bonding of the ruthenium to both the zeolite surface and the acac ligands. The Ru−C contribution is consistent with the IR and mass spectrometry data indicating ethylene ligands, and the Ru−C coordination number of ∼4 indicates the presence of two such ligands per Ru atom. The Ru−C distance essentially matches the crystallographic results characterizing the precursor complex **I** (2.183−2.212 Å). The Ru−Al contribution, at a distance of 3.08 Å with a coordination number of ∼1, indicates, as expected, that the cationic complex **I** reacted with the zeolite to give a cationic complex bonded to sites where acidic silanol groups had been present. Thus, the structure of the supported complex represented below is in accord with all of the data.

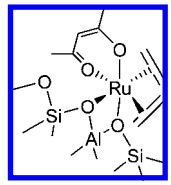

The Ru−C contribution with a coordination number of ∼2 at a distance of 3.03 Å (Table 1) was attributed to the two carbonyl carbons in the acac ligand remaining on the ruthenium (see the Discussion). The distance is longer than that observed in the precursor **I** (∼2.93−2.98 Å, as estimated from crystallographic data[28]), suggesting that the precursor and the supported complex are not very close analogues.

Summary of EXAFS Fitting. In summary, the EXAFS results indicate that the supported species was a cationic, mononuclear diethylene ruthenium complex anchored tightly to the surface at Al^{3+} sites by Ru−O bonds. The IR data reinforce this model, as described further in the Discussion.

Catalytic Dimerization of Ethylene. Blank Experiments. Flow-reactor experiments were conducted with the bare zeolite and with structures formed from adsorption of $Ru(acac)_3$ on the zeolite. No detectable conversion of C_2H_4 (or $C_2H_4 + H_2$) was observed at room temperature with either of these samples.

Reaction Products and Activity of the Catalyst. In contrast, the supported ruthenium complex (Sample 1) was catalytically active and gave mixtures of butenes with a trace amount of ethane (<0.05% of the total product) when the feed to the flow reactor was an equimolar mixture of C_2H_4 and H_2 at room temperature. Ethylene conversions were <5% at steady state, mostly ranging from 1 to 3%. Therefore, the reactor was treated as differential, and the reaction rate (turnover frequency, TOF) was determined directly from the conversion data. Higher conversions were also measured but are not reported here.

Figure 5A,B shows TOF and butene selectivity data as a function of time on stream with a feed mixture containing C_2H_4 and H_2 at room temperature, each at a partial pressure of 4 kPa in helium, at a total pressure of 101 kPa. The TOF was nearly independent of time on stream under these conditions. The butene selectivity changed slightly at the beginning of the flow-

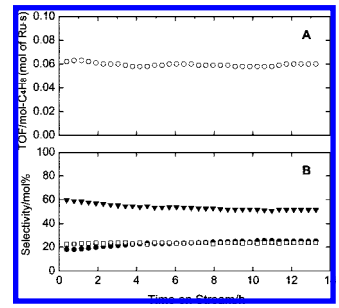

Figure 5. Catalysis of ethylene dimerization in a flow reactor: (A) TOF and (B) butene selectivity [(▼) *trans*-2-butene, (•) 1-butene, (□) *cis*-2-butene] as functions of time on stream. Feed composition: 4/4/93 C_2H_4/H_2/He. Total flow rate: 100 mL (NTP)/min.

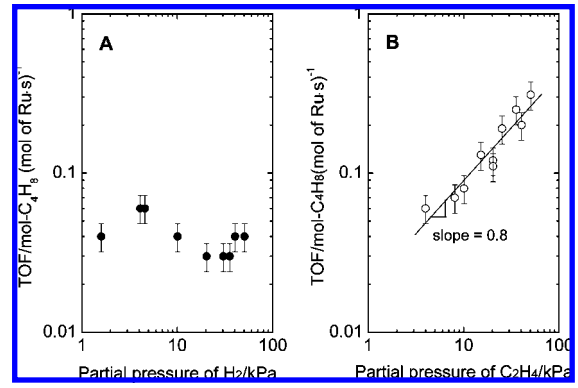

Figure 6. Kinetics data: TOF as a function of the partial pressure of (A) H_2 (with $P_{C_2H_4} = 4$ kPa) and (B) C_2H_4 (with $P_{H_2} = 4$ kPa). Other conditions: $P_{total} = 101$ kPa (balance He); room temperature.

reactor experiment and reached a near-steady state (with a 1-butene/*trans*-2-butene/*cis*-2-butene molar ratio of 23/52/25) after ∼11 h.

The TOF in the near-steady state was 0.06 mol of C_4H_8 (mol of Ru)$^{-1}$ s^{-1}. The number of turnovers was 2800 when the experiment was stopped after reaction for ∼14 h; clearly, the reaction was catalytic.

Increasing the C_2H_4 partial pressure led to increased selectivity for 1-butene formation. For example, an increase in the C_2H_4 partial pressure from 4 to 51 kPa at a H_2 partial pressure of 4 kPa and a total pressure of 101 kPa led to an increase in the selectivity for 1-butene formation from 23 to 92% as the selectivities for *trans*-2-butene and *cis*-2-butene each decreased to 4%.

Although ethylene dimerization might be expected to proceed without H_2,[50−55] the reaction was much slower without H_2 in the feed stream (TOF ≈ 1 × 10^{-4} s^{-1}), and then gave 1-butene as the only detectable product. Thus, H_2 played a role in forming the catalytically active species.

Figure 6A,B shows values of the TOF at near-steady state as functions of the partial pressures of the reactants. The errors shown on the plot were attributed primarily to uncertainties in weighing of the catalyst in the glovebox. As described above,

(50) Laurenczy, G.; Merbach, A. E. *J. Chem. Soc., Chem. Commun.* **1993**, 187.
(51) Yashima, T.; Ebisawa, M.; Hara, N. *Chem. Lett.* **1972**, 473.
(52) Bass, J. S.; Kevan, L. *J. Phys. Chem.* **1990**, *94*, 1483.
(53) Hartmann, M.; Pöppl, A.; Kevan, L. *J. Phys. Chem.* **1996**, *100*, 9906.
(54) Takahashi, N.; Okura, I.; Keii, T. *J. Am. Chem. Soc.* **1975**, *97*, 7489.
(55) Baba, T.; Nakano, K.; Nishiyama, S.; Tsuruya, S.; Masai, M. *Appl. Catal.* **1989**, *52*, 81.

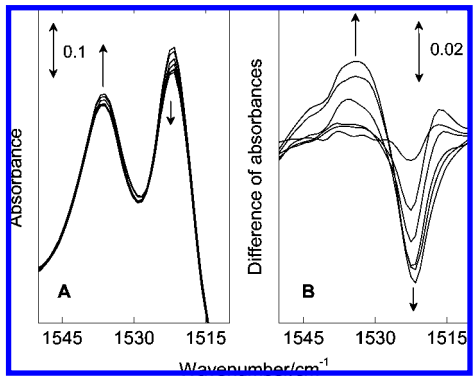

Figure 7. Time evolution of (A) IR spectra recorded at the start of the catalytic reaction in a flow reactor and (B) the corresponding difference spectra. The arrows indicate the directional changes of the absorbances of individual peaks as a function of time.

H_2 was required for the catalyst to initiate the reaction. As Figure 6A shows, the rate increased with increasing H_2 partial pressure up to ~4 kPa and then decreased at higher H_2 partial pressures. This decrease suggests inhibition by H_2. On the other hand, the TOF increased monotonically with increasing C_2H_4 partial pressure; the reaction order with respect to C_2H_4 was 0.8 (Figure 6B).

In contrast to the zeolite-supported Sample 1, the silica-supported ruthenium sample was characterized by only a low activity (TOF = 7×10^{-3} s^{-1}), even in the presence of H_2 (C_2H_4 and H_2, each at 4 kPa, in He). This result suggests that catalytically active species barely formed on the amorphous silica support, and a comparison of the two catalysts suggests that Al^{3+} sites in the zeolite might be responsible for creating catalytically active species.

IR Spectra of the Working Catalyst. To understand the roles of H_2 and zeolite Al^{3+} sites in the genesis of the catalytically active species, experiments were conducted under the same flow conditions stated above (C_2H_4 and H_2, each at a partial pressure of 4 kPa, in He; 100 mL/min total flow) with 30 mg of the sample in an IR cell serving as a flow reactor.

Figure 7 shows the changes in the IR bands characteristic of acac ligands bonded to aluminum sites (Al−acac) and to ruthenium sites (Ru−acac) during the catalysis. The intensity of the Ru−acac band decreased and that of the Al−acac band began to increase when the flow of reactants started, suggesting that dissociation of acac ligands from ruthenium and their subsequent bonding to Al^{3+} sites in the zeolite yielded the catalytically active species.

Discussion

Chemistry of Chemisorption of the Precursor Complex I on the Zeolite. The IR data (Figure 3) showed that some of the acac ligands were dissociated from the ruthenium after chemisorption of **I** on the zeolite. The fraction of the acac ligands dissociated from the ruthenium was estimated from the IR spectra by deconvolution according to the Pearson VII model[56−58] (as described in the Supporting Information). The deconvolution was implemented by choosing five peaks (centered at 1521, 1537, 1555, 1575, and 1590 cm^{-1}) and applying Levenberg−Marquardt iterations to optimize the parameters. The peak deconvolution (assuming the same molar extinction coefficient for each species) gave an Al−acac/Ru−acac area ratio of 49/51 for Sample 1, which contained 1 wt% Ru (see Figure 10S in the Supporting Information), showing that essentially half of the acac ligands were dissociated from the ruthenium and bonded to Al^{3+} sites. This result was further supported by the EXAFS data: the bonding Ru−O contribution with a coordination number of ~4 corresponds to two O atoms of one acac ligand and two O atoms of the zeolite, and the long Ru−C contribution (Ru−C_l) with a coordination number of ~2 arises from two carbonyl carbons per acac ligand. The Ru−C_l contribution was characterized by a longer distance (3.03 Å) than the crystallographic value characterizing the precursor,[28] indicating a distortion of the structure from that in the precursor **I**.

Chemistry of Adsorption of I with Samples Containing 2 or 3 wt % Ru. On the basis of these results, we inferred that one precursor molecule **I** reacted with two Al^{3+} sites (one for anchoring the ruthenium complex and one for bonding to a dissociated acac ligand) and that all of the ruthenium complexes in this sample were dissociated and chemisorbed. By inference, we expected a maximum loading of one chemisorbed ruthenium complex per two Al atoms.

To approximately determine the value of this maximum by experiment, we also investigated samples with higher ruthenium loadings (2 and 3 wt%). The Al−acac/Ru−acac area ratios determined from IR spectra characterizing these samples were found to decrease with increasing ruthenium loading. Peak deconvolutions of the Ru−acac and Al−acac bands, determined as mentioned above, yielded Al−acac/Ru−acac ratios of 24/76 and 18/82, respectively, for the samples containing 2 and 3 wt% Ru, respectively (Figures 12S and 13S in the Supporting Information). Thus, the samples with Ru loadings of 2 and 3 wt % were characterized by lower Al−acac/Ru−acac ratios than the sample containing 1 wt % Ru, demonstrating the presence in the former samples of some ruthenium complexes that did not exchange acac ligands with the zeolite. Thus, the experiments confirmed that the maximum loading for dissociative chemisorption of the ruthenium complex was in the range of 1−2 wt % Ru and that the available Al^{3+} sites were saturated in the samples containing 2 and 3 wt % Ru. Some of the ruthenium complexes in these samples were evidently physisorbed, with the acac ligands retained by the ruthenium.

Because Sample 1 contained approximately one ruthenium complex per six Al atoms and an amount of chemisorbed ruthenium complex that did not exceed the maximum value, we infer that not all of the Al^{3+} sites in the zeolite were accessible to **I** or that some of the Al^{3+} sites were nonframework sites[59] and might not be suitable for anchoring the complexes; the inaccessible sites were presumably in the β-cages, as characterized by IR bands at 3565 cm^{-1} (Figure 1).

To determine the value of maximum loading for chemisorption of the ruthenium more exactly, we performed the following approximate analysis:

If we assume that the maximum loading of Ru to form chemisorbed ruthenium complexes is 1 wt %, then x wt % Ru ($x > 1$) would result in 1 wt % chemisorbed complexes and ($x - 1$) wt % physisorbed species. This assumption would lead to a value of $1/(2x)$ for the area ratio Al−acac/(Al−acac +

(56) Elderton, W. P; Johnson, N. L. *Systems of Frequency Curves*; Cambridge University Press: London, 1969.
(57) Chen, L.; Garland, M. *Appl. Spectrosc.* **2003**, *57*, 331.
(58) Bhan, A.; Allian, A. D.; Sunley, G. J.; Law, D. J.; Iglesia, E. *J. Am. Chem. Soc.* **2007**, *129*, 4919.
(59) Shannon, R. D.; Gardner, K. H.; Staley, R. H.; Bergeret, G.; Gallezot, P.; Auroux, A. *J. Phys. Chem.* **1985**, *89*, 4778.

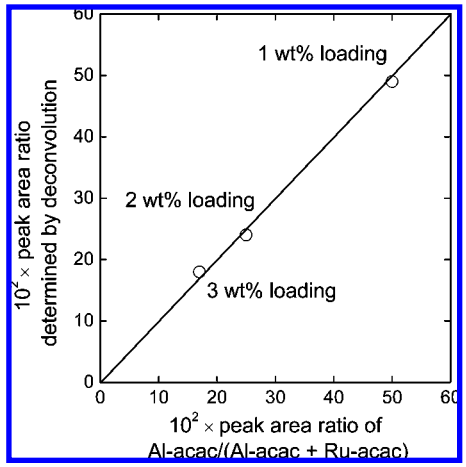

Figure 8. Values of the peak-area ratio Al−acac/(Al−acac + Ru−acac) determined by deconvolution of IR spectra vs those calculated on the basis of the assumption that the maximum loading of ruthenium is 1 wt%.

Ru−acac). The area ratios for the three samples with different Ru loadings were calculated and compared with those determined from the IR data (Figure 8). The agreement is good, pointing to the validity of the assumption. Thus, we conclude that the maximum loading of Ru is ∼1 wt%.

Structural Model of the Supported Ruthenium Complex. On the basis of the IR and EXAFS data representing Sample 1, we infer that chemisorption of the precursor **I** led to the replacement of one acac ligand per Ru atom with two oxygen atoms of the support, producing the surface-bound species shown in the structural model given in the Results.

The surface-bound species modeled in this structure is formally a coordinatively saturated 18-electron species if one assumes that the surface oxygen atoms are two-electron donors (i.e., assuming a formal charge of −1 on an AlO_2 unit): 6 e^- for Ru(II), 4 e^- for acac, 4 e^- for the zeolite oxygen ligand, and 4 e^- for the two ethylene ligands. The implications of the coordinative saturation in regard to catalysis are presented below.

Reaction of the Supported Ruthenium Complex to Enter the Catalytic Cycle. If the proposed structural model of the surface species in the initially prepared sample (Sample 1) is valid, ligand dissociation must take place for this species to enter the catalytic ethylene dimerization cycle. This reaction proceeded much faster with a cofeed of C_2H_4 and H_2 than without H_2. This result suggests that H_2 played a role in the creation of the catalytically active species, as indicated by the IR data (Figure 7).

Several ruthenium(II) complexes in solution have been reported to enter catalytic cycles through the dissociation of ligands via heterolytic cleavage of H_2.[60] The ruthenium complexes in these examples stay in the same formal oxidation state (II, d^6 metal). For example, $RuCl_2(PPh_3)_3$[17] was reported to react with H_2 as H_2 is activated heterolytically, forming $RuHCl(PPh_3)_3$ and HCl.[61] A precatalyst for asymmetric hydrogenation, $Ru(CH_3COO)_2$[BINAP], is believed to enter a catalytic cycle via dissociation of an CH_3COO^- ligand as CH_3COOH and coordination of a hydride, producing the catalytically active $Ru(CH_3COO)(H)$[BINAP].[62−65]

As these examples imply, the surface ruthenium species of the as-prepared Sample 1 may enter into a catalytic cycle via (1) heterolytic cleavage of H_2 into a proton and a hydride on the ruthenium complex, (2) protonation of the acac ligand, (3) dissociation of the protonated acac ligand (the enol form of $C_5H_8O_2$), (4) coordination of the acetylacetone to an Al site of the zeolite and deprotonation of the resultant species, and (5) protonation of an oxygen atom of the zeolite bonded to the Al site.

Conclusions

Zeolite-supported ruthenium complexes were prepared by the reaction of **I** with dealuminated zeolite Y. The high degree of structural uniformity of the supported species[10] allowed a detailed characterization of the chemistry of the supported complex, including the bonding of the ruthenium to the support surface. Precursor **I** reacted with acidic silanol groups on the surface of the zeolite as one of two acac ligands in **I** was dissociated from the ruthenium and bonded at an aluminum site in the zeolite, and the ethylene ligands were retained by the ruthenium. After this reaction, the ruthenium complexes remained mononuclear, becoming bonded to the site where acidic silanol groups had been present. The maximum loading of ruthenium on the zeolite as chemisorbed species is ∼1 wt %. The supported metal complex with 1 wt % loading of ruthenium catalyzed ethylene dimerization at room temperature. H_2 facilitated the formation of the catalytically active species by inducing the dissociation of acac ligands from ruthenium; the dissociated acac ligands were scavenged by aluminum sites in the zeolite.

Experimental Methods

Materials and Procedures. Sample handling was carried out with standard Schlenk techniques, and samples were prepared and stored in a glovebox under dry Ar. Glassware was dried at 120 °C overnight prior to use in syntheses. Immediately before use in syntheses, *n*-pentane solvent was distilled from Na/benzophenone and then deoxygenated by sparging of N_2. $Ru(acac)_3$ (Strem, 99%), was used to synthesize **I**. He, H_2, and C_2H_4 (all Airgas, UHP grade) were purified by passage through traps containing activated zeolite 4A and reduced Cu/Al_2O_3 to remove traces of moisture and O_2, respectively. D_2 (Cambridge Isotopes, 99.6% D_2 + 0.4% HD) was used as received. Dealuminated zeolite HY [Zeolyst, CBV760, Si/Al ratio = 30 (atomic)] and silica (Degussa, Aerosil 200) were used as supports.

Synthesis of the Ruthenium Complex Precursor I. The ruthenium complex **I** was synthesized by a literature method,[28] and the ^1H and ^{13}C NMR spectra and IR spectra essentially matched the literature values, as follows: ^1H NMR (500 MHz, C_6D_6): δ 5.26 (s, 2H, γ-CH), 3.72−3.87 (m, 8H, C_2H_4), 1.84, 1.88 (each s, 6H, CH_3). ^{13}C NMR (500 MHz, C_6D_6): δ 187.2 (C═O), 185.7 (C═O), 98.7 (γ-C), 78.7 (C_2H_4), 28.1 (CH_3), 27.5 (CH_3). IR (KBr): 1576, 1515 cm^{-1} (acac).

Synthesis of Zeolite-Supported Ruthenium Complexes. The zeolite was calcined by heating from room temperature to 773 K in flowing dry O_2 over a period of 3 h followed by a period of constant temperature (773 K) for 4 h in flowing O_2 and then 16 h

(60) Kubas, G. J. *Chem. Rev.* **2007**, *107*, 4152.
(61) Crabtree, R. H. *The Organometallic Chemistry of the Transition Metals*, 4th ed.; Wiley-Interscience: Hoboken, NJ, 2005; p 251.
(62) Kitamura, M.; Tsukamoto, M.; Bessho, Y.; Yoshimura, M.; Kobs, U.; Widhalm, M.; Noyori, R. *J. Am. Chem. Soc.* **2002**, *124*, 6649.
(63) Noyori, R.; Kitamura, M.; Ohkuma, T. *Proc. Natl. Acad. Sci. U.S.A.* **2004**, *101*, 5356.
(64) Wiles, J. A.; Bergens, S. H.; Young, V. G. *J. Am. Chem. Soc.* **1997**, *119*, 2940.
(65) Ashby, M. T.; Halpern, J. *J. Am. Chem. Soc.* **1991**, *113*, 589.

under vacuum. The zeolite under vacuum was then cooled to room temperature and used immediately for sample preparation, as follows:

To 2.0 g of calcined zeolite in a 100 mL Schlenk flask with a stir bar was added 0.072 g of complex **I** [Ru/Al ≈ 1/6 (atomic)]. To this mixture was added ∼30 mL of freshly distilled *n*-pentane. The mixture was stirred at room temperature, and after 18 h, the *n*-pentane was removed by evacuation.

Samples with higher ruthenium loadings were prepared similarly. A zeolite-supported sample prepared from $Ru(acac)_3$ was prepared similarly, using $Ru(acac)_3$ instead of **I** as the precursor. A silica-supported sample was prepared similarly by using silica instead of the zeolite. The ruthenium loading was 1 wt %.

Acetylacetone Adsorbed on Zeolite. To 1.2 g of calcined zeolite in a 50 mL Schenk flask with a stir bar was added ∼20 mL of freshly distilled *n*-pentane; 0.012 g of acetylacetone (Aldrich, 0.12 mmol) was added to this mixture by syringe. The resultant mixture was stirred for 18 h at room temperature, and the solvent was then removed by evacuation.

Ethylene Dimerization Catalysis. The zeolite-supported sample was tested as a catalyst with a reactant mixture consisting of ethylene, H_2, and He. The reaction was performed in a once-through flow reactor (i.d. = 1.0 cm). The supported sample (10 mg) was diluted with 6 g of inert, nonporous α-Al_2O_3 (Fisher) in a glovebox and then loaded into the reactor and transferred to the flow system without coming into contact with air. The partial pressures of ethylene and H_2 were varied individually, and the total pressure was atmospheric. The flow rate of the feed mixture was maintained at 100 mL (NTP)/min by adjusting the helium flow rate when the composition was changed.

Products were analyzed by gas chromatography using an HP-6890 gas chromatograph equipped with a 50 m × 0.53 mm DB-624 capillary column (J & W Scientific) and an FID detector. In a typical run, ethylene and H_2, each at a partial pressure of 4.0 kPa, flowed through the catalyst bed. The effluent gas was sampled every 30 min and analyzed. The ethylene conversions were <5%, and the reactor was treated as differential.

NMR Spectroscopy of the Ruthenium Complex Precursor. NMR spectra were recorded at 293.6 K with a Bruker Avance 500 spectrometer (^1H at 500 MHz, ^{13}C at 125.8 MHz). The chemical shifts (δ) for ^1H and ^{13}C are given in parts per million referenced to the residual solvent peaks (7.16 ppm for ^1H and 128.06 ppm for ^{13}C, C_6D_6, Aldrich 99.5%).

IR Spectroscopy of Zeolite-Supported Ruthenium Complexes and Analysis of Effluent Gases. Spectra were collected in transmission mode with a Bruker IFS 66v Fourier transform spectrometer with a spectral resolution of 2 cm^{-1}. The solid sample, a pressed wafer, was held at room temperature under dynamic vacuum ($<10^{-4}$ kPa). Each spectrum was the average of 64 scans. In some experiments, the sample was in contact with flowing gas; ∼30 mg of the solid sample in the glovebox was loaded into a cell that served as a flow reactor (In-situ Research Institute, Inc., South Bend, IN). The cell was sealed and connected into a flow system that allowed recording of spectra while the reactant gases flowed through the cell at the reaction temperature. In experiments with D_2, ∼5 mL of D_2 was pulsed into a stream of He flowing at 100 mL/min through the cell at room temperature.

IR spectra were baseline-corrected with OPUS software (Bruker). Deconvolution of the IR spectra was implemented using the Pearson VII model (the equation is shown in the Supporting Information). The fit parameters were optimized by Levenberg−Marquardt iterations.

The effluent gas was analyzed by mass spectrometry (Pfeiffer Vacuum, Omni Star).

X-ray Absorption Spectroscopy of Supported Ruthenium Complexes. Ru K-edge X-ray absorption spectra were measured at the Stanford Synchrotron Radiation Laboratory (SSRL) on the unfocused 30-pole 1.45 T wiggler beam line 10−2 under standard ring operating conditions, with a storage-ring electron energy of 3 GeV and a ring current of 60−100 mA. A Si(220) double-crystal monochromator was used for selection of the beam energy. The monochromator was detuned to 75% of maximum intensity to reduce the interference of higher harmonics present in the X-ray beam.

The mass of each sample was chosen to give an absorbance between 1.5 and 3.0 calculated at 50 eV above the absorption edge. The sample was placed in a cell[66] and maintained under vacuum ($<10^{-7}$ kPa) at liquid nitrogen temperature during the data collection. X-ray intensity data were collected in transmission mode by use of ion chambers mounted on each end of the sample cell. The energy was calibrated by simultaneous measurement of the absorption of a ruthenium metal foil. The beam exiting the ring first passed through an ion chamber containing N_2, and then through the sample cell, an ion chamber containing argon, a cell containing the ruthenium foil, and finally an ion chamber containing argon. Data were measured at values of the wave vector k up to 16 $Å^{-1}$. The first inflection point of the spectrum of the foil was assigned to be 22117 eV. The EXAFS data analysis procedure is summarized in detail in the Supporting Information.

Acknowledgment. This research was supported by the U.S. Department of Energy, Office of Energy Research, Basic Energy Sciences Grant FG02-04ER15513. We acknowledge beam time and the support of the DOE Division of Materials Sciences for its role in the operation and development of beam line 10−2 at the Stanford Synchrotron Radiation Laboratory, and we thank the beam line staff. We also thank Dr. Y. Ping of the University of California, Davis, for collecting solution NMR data.

Note Added after ASAP Publication. After this paper was published ASAP September 12, 2008, the formula for the mononuclear ruthenium complex was corrected in two places in the Abstract. The corrected version was published October 1, 2008.

Supporting Information Available: EXAFS data analysis procedure, ^1H and ^{13}C NMR spectra of **I**, IR spectra of zeolite-supported ruthenium complexes, IR spectrum of a silica-supported ruthenium complex, Fourier transforms of EXAFS data, and IR spectra and their deconvolutions. This material is available free of charge via the Internet at http://pubs.acs.org.

JA804265R

(66) Jentoft, R. E.; Deutsch, S. E.; Gates, B. C. *Rev. Sci. Instrum.* **1996**, *67*, 2111.